Journal of Colloid and Interface Science 552 (2019) 439–447

Contents lists available at ScienceDirect

Journal of Colloid and Interface Science

journal homepage: www.elsevier.com/locate/jcis

Regular Article

pH-responsive dithiomaleimide-amphiphilic block copolymer for drug delivery and cellular imaging

Ting Bai [a], Dongyan Shao [b], Jianxin Chen [a], Yifan Li [c], Ben Bin Xu [c,*], Jie Kong [a,*]

[a] Shaanxi Key Laboratory of Macromolecular Science and Technology, School of Science, Northwestern Polytechnical University, Xi'an 710072, PR China
[b] Key Laboratory for Space Bioscience and Biotechnology, School of Life Sciences, Northwestern Polytechnical University, Xi'an 710072, PR China
[c] Mechanical and Construction Engineering, Faculty of Engineering and Environment, Northumbria University, Newcastle upon Tyne NE1 8ST, UK

GRAPHICAL ABSTRACT

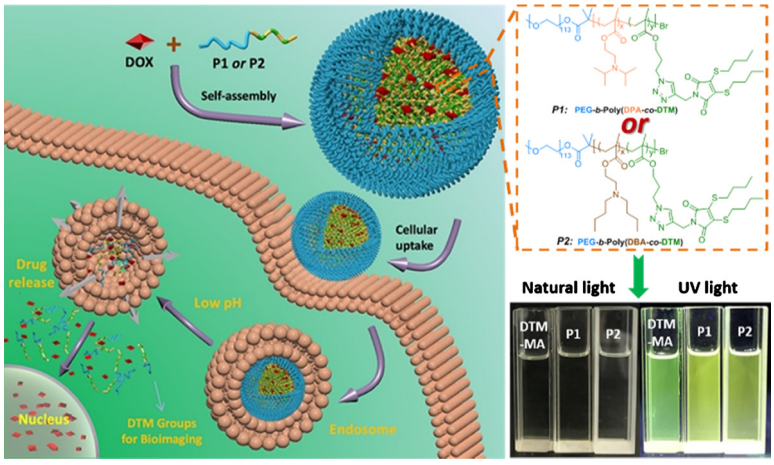

ARTICLE INFO

Article history:
Received 25 February 2019
Revised 21 May 2019
Accepted 22 May 2019
Available online 23 May 2019

Keywords:
Dithiomaleimide
Fluorescence imaging
pH-responsive
Amphiphilic block copolymer
Drug delivery

ABSTRACT

A drug delivery system that is integrated with fluorescent imaging is an emerging platform for tumor diagnostic and therapy. A pH-responsive fluorescent polymer that can respond to the surrounding medium is a desired component with which to construct an advanced drug delivery system with bioimaging characteristics and controllable drug releasing. In this work, we synthesized novel amphiphilic block copolymers of poly(ethylene glycol)-*b*-poly(2-(diisopropylamino) ethyl methacrylate-*co*-dithiomaleimide) (PEG-*b*-poly(DPA-*co*-DTM)) and poly(ethylene glycol)-*b*-poly(2-(dibutylamino) ethyl methacrylate-*co*-dithiomaleimide) (PEG-*b*-poly(DBA-*co*-DTM)) with pH-responsiveness and fluorescence. The block copolymers exhibited relatively stable fluorescence properties in different solvent and excitation-independent fluorescence behaviours. By copolymerizing the responsive segments in the molecule chain, the doxorubicin (DOX)-loaded micelles could be triggered to disassemble, thus releasing DOX at the corresponding pH values and yielding a pH-responsive drug release. Targeted deliveries of the drug within the cell were demonstrated by using the carrier responding to different pH values. The best antitumor effect was obtained by PEG-*b*-poly(DPA-*co*-DTM), which immediately released DOX as soon as it entered the tumor cells, as a result of responding to the regional pH level (pH = 6.3). The pH-responsive copolymers showed excellent biocompatibilities, as nearly 85% of cells with these fluorescent micelles survive when the testing concentration goes up to 200 μg mL^{-1}. In all, these pH-responsive and

* Corresponding authors.
E-mail addresses: ben.xu@northumbria.ac.uk (B.B. Xu), kongjie@nwpu.edu.cn (J. Kong).

https://doi.org/10.1016/j.jcis.2019.05.074
0021-9797/

dithiomaleimide-based fluorescent block copolymers hold great potential in future cancer diagnostic and therapeutic techniques.

1. Introduction

Fluorescence imaging, which is a reliable strategy to detect and visualize biosubjects both *in vitro* and *in vivo* [1–3], has led to wide applications in clinical practices [4–7]. The key features for the fluorescence imaging technique, which is normally driven by a high specification fluorescent probe, have high sensitivity and nonradioactivity [1,8], which can acquire feedback and good biocompatibility at molecular level [1]. Recent developments on quality fluorescence imaging suggested a few technical bottlenecks, i.e., aggregation-caused quenching of traditional organic fluorophores [9–11], cytotoxicity of semiconductor quantum dots [12,13], and a low luminescence intensity of lanthanide luminescent materials [3]. Therefore, there is a current demand to enhance and/or seek novel fluorescent probes to address the above technical gaps. At the same time, most of the above mentioned probes occupy poor water solubility and a short circulation time, so many polymer-based micelle systems have been developed for the transportation of bioimaging probes [14]. For example, Zhu's group reported a glucose-based NIR-fluorescence polymer, PMMA-*b*-P(GATH-*co*-BOD), for cancer detection with a strong recognition towards GLUT1 [15].

In addition, combining bioimaging with smart drug release to obtain multifunctional nanomaterials is of great significance in diagnostic and therapeutic applications [16,17]. These imaging-guided drug delivery systems can visualize the accumulation of nanoparticles and simultaneously deliver and trace the drug, thereby evaluating the efficiency of drug delivery [17,18]. For molecular therapies, these nanomaterials may be able to understand the pharmacokinetic processes that are important in nanomedicine [18]. Therefore, fluorescent and pH-responsive polymers are popular in imaging-guided drug delivery systems. These responsive nanoparticles are able to recognize the small pH changes around the tumor microenvironment, where the pH value in early endosomes is approximately 5.9–6.2, but is approximately 5.0–5.5 in the late endosomes/lysosomes [19–23]. However, an advanced drug delivery strategy with high pH sensitivity and fast responsiveness remains to be fully exploited.

From the perspective of scoping novel materials, the poly(2-(diisopropylamino) ethyl methacrylate) (PDPA) and poly(2-(dibutylamino) ethyl methacrylate) (PDBA) are found to be highly sensitive to pH in early endosomes and in late endosomes/lysosomes, which envisage their potential in controlled drug delivery applications [24–29]. Dithiomaleimides (DTMs) are a class of highly emissive fluorophores that possess a smart ON-OFF emissive switch effect [30,31], that can be copolymerized into a fluorescence polymer-DTM [32–35] with applications in proteins-labeling [30,36], gene delivery [30] and controlled drug release [37].

In this work, we propose a novel fluorescent and pH-responsive material strategy by copolymerizing fluorescent DTM groups with pH-sensitive polymers (PDPA and PDBA), thereby aiming to improve the efficiency for cell imaging and drug release. The drug release roadmap is shown in Scheme 1. The DOX-loaded micelles that were self-assembled from PEG-*b*-poly(DPA-*co*-DTM) or PEG-*b*-poly(DBA-*co*-DTM) were taken up by tumor cells, and the pH-responsive parts became positively charged at a low pH, thus leading to the dissociation of micelles into unimers and releasing DOX. Simultaneously, the DTM probes exhibited bright green fluorescence to achieve cellular imaging.

2. Experimental

2.1. Materials

The 2,3-dibromomaleimide (98%) was purchased from Ark. Butanethiol (97%) was purchased from TCI. Propargyl bromide (98%, contains 0.3% MgO as a stabilizer), 2-bromo-2-methylpropionyl bromide (98%), 3-chloro-1-propanol (98%) and *N,N,N′,N′,N″*-pentamethyl-diethylenetriamine (PMDETA, 99%) and trimethylamine (TEA, 99.7%) were purchased from Aladdin. 2-Diisopropylaminoethanol (98%) was purchased from Adamas. Poly(ethylene glycol) methyl ether (PEG_{113}-OH, M_n = 5000) and 2-(dibutylamino)ethanol (99%) were purchased from Aldrich and were used as received. A549 cell lines were purchased from the China Center for Type Culture Collection (Wuhan, China). Dulbecco's modified Eagle medium (DMEM) was purchased from HyClone. Fetal bovine serum (FBS), phosphate buffered saline (PBS) and Cell Counting Kit-8 were purchased from Beyotime. All other reagents were available commercially from J&K Chemical and were used as received. Alkyne-DTM [38,39], 3-azido propanol (AzPOH) [40,41], 3-azidopropyl methacrylate (AzPMA) [40,41], 2-(diisopropylamino)ethyl methacrylate (DPA-MA) and 2-(dibutylamino)ethyl methacrylate (DBA-MA) [25], as well as PEG-Br [29] were synthesized according to a previously reported method.

2.2. Synthesis of methacrylate-functional DTM (DTM-MA)

DTM-MA was synthesized via the "click" reaction. Alkyne-DTM (934.14 mg, 3 mmol), AzPMA (558.13 mg, 3.3 mmol) and PMDETA (138.4 mg, 0.8 mmol) were dissolved in 5 mL anhydrous dimethylformamide (DMF). The mixture was degassed via three freeze-evacuate-thaw cycles followed by the addition of CuBr (114.8 mg, 0.8 mmol). The solution was allowed to be stirred for 24 h under N_2 atmosphere at 50 °C. Then, the solution was exposed to air and was diluted with dichloromethane (DCM). The mixture was then passed through a neutral alumina, and the residue was purified by silica gel column chromatography (hexane:ethyl acetate = 2:1, v/v) to yield yellow liquid (1.2 g, 83%). ^{1}H NMR (400 MHz, $CDCl_3$) δ: 0.93 (—S—$(CH_2)_3$—C***H***$_3$), 1.44 (—S—$(CH_2)_2$—C***H***$_2$—CH_3), 1.63 (—S—CH_2—C***H***$_2$—CH_2—CH_3), 1.95 (CH_2=C(CH_3)—), 2.31 (—O—CH_2—C***H***$_2$—CH_2—), 3.3 (—S—C***H***$_2$—$(CH_2)_2$—CH_3), 4.2 (—O—C***H***$_2$—), 4.45 (—O—$(CH_2)_2$—C***H***$_2$—), 4.81 (—CH=CH(C***H***$_2$)—), 5.62, 6.11 (C***H***$_2$=C(CH_3)—), 7.58 (triazole).

2.3. Synthesis of PEG-b-poly(DPA-co-DTM) and PEG-b-poly(DBA-co-DTM) block copolymers

PEG-*b*-poly(DPA-*co*-DTM) and PEG-*b*-poly(DBA-*co*-DTM) block copolymers of different compositions were synthesized by atom transfer radical polymerization (ATRP). The synthesis of PEG-*b*-poly(DPA-*co*-DTM) was described as a representative procedure. PEG-Br (100 mg, 0.02 mmol), DPA-MA (170.65 mg, 0.8 mmol), DTM-MA (48.05 mg, 0.1 mmol) and PMDETA (3.46 mg, 0.02 mmol) were dissolved in 2 mL anhydrous DMF. The mixture was degassed via three freeze-evacuate-thaw cycles followed by the addition of CuBr (2.87 mg, 0.02 mmol). After 12 h of stirring under an N_2 atmosphere at 60 °C, the reaction bottle was quickly quenched into an ice bath and exposed to air, then diluted with DCM. The mixture

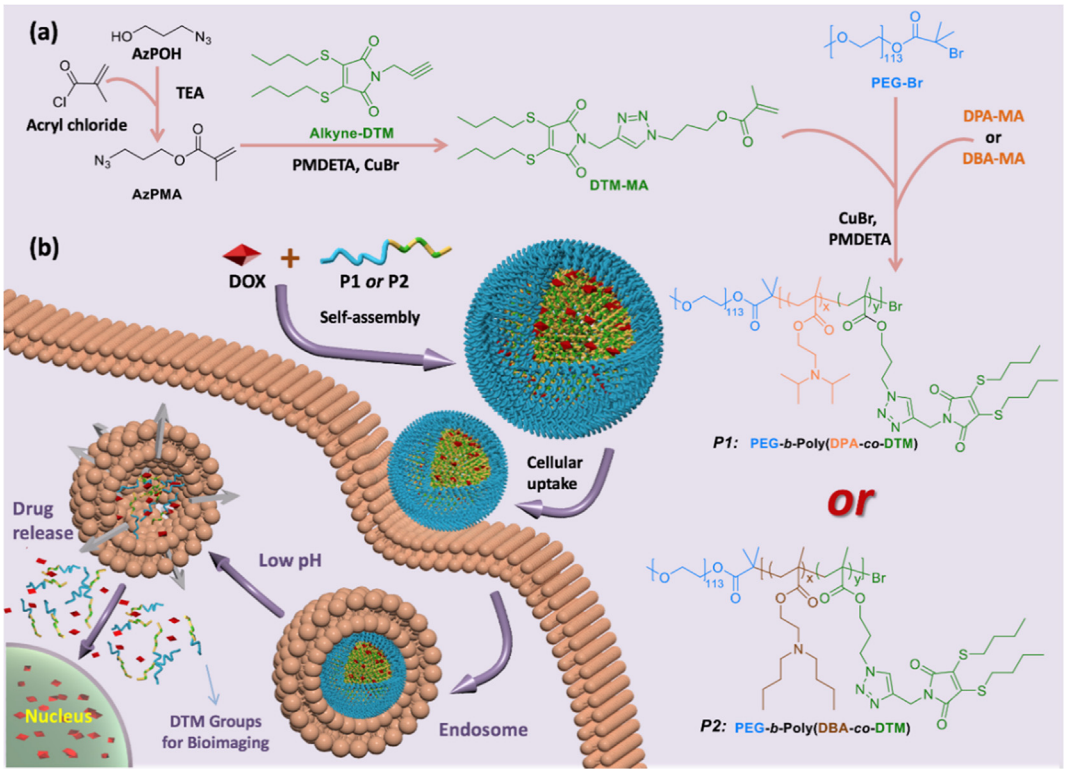

Scheme 1. Schematic for the preparation of fluorescent dithiomaleimide-amphiphilic block copolymers, PEG-*b*-poly(DPA-*co*-DTM) and PEG-*b*-poly(DBA-*co*-DTM) (a), and an illustration of pH-responsive drug delivery into a tumor cell (b).

was then passed through a neutral alumina. The filtrate was concentrated twice and precipitated into excess cold diethyl ether, then dried in a vacuum to yield a yellowish-brown solid.

2.4. Characterization

^{1}H NMR spectra were recorded on a Bruker AV 400 NMR spectrometer with $CDCl_3$ as the solvent. Fourier transform infrared spectra (FT-IR) were recorded using a NICOLET iS10 IR spectrometer using the potassium bromide (KBr) method. The number- and weight-average molecular weight (M_n and M_w, respectively) and the polydispersity index (PDI = M_w/M_n) were measured using a GPC-MALLS system equipped with a Waters 515 pump, an autosampler and two gel columns (10^3 Å and 10^4 Å, MZ, Shimadzu Co.) at a flow rate of 0.5 mL min^{-1} in THF (HPLC grade) at 25 °C. The detectors that were used included a differential refractometer (Optilab rEX, Wyatt) and a multiangle light scattering detector (MALLS) equipped with a 632.8 nm He-Ne laser (DAWN EOS, Wyatt). The refractive index increments (d*n*/dc) of polymers in the THF were measured at 25 °C using an Optilab rEX differential refractometer. ASTRA software (Version 5.1.3.0) was utilized for the acquisition and analysis of data. At the adjustment stage of this instrument, the polystyrene standard was used. Dynamic light scattering (DLS) measurements were made with a Zetasizer Nano-ZS (Malvern Instruments, UK). Cryo-transmission electron microscopy (cryo-TEM) was performed with an FEI Talos F200C microscope (Thermo Scientific, US) with an electron kinetic energy of 200 kV. The samples were prepared by dropping micelle solutions onto copper grids, which were allowed to immediately freeze in liquid N_2 overnight before measurement. The fluorescence spectra of compounds were measured on a Hitachi F-4500 spectrophotometer equipped with a 150 W xenon lamp as the excitation source, and both slit widths were set at 5 nm for excitation and emission. The cell uptake experiment was conducted by confocal microscopy (Leica TCS-SP5). Cell viability was detected by M200 Pro nanoquant (Tecan). The cell apoptosis was evaluated by a Muse Cell Analyzer (Merck & Millipore, Germany).

2.5. Preparation of micelle nanoparticles

Micelles were prepared by a dialysis method. PEG-*b*-poly(DPA-*co*-DTM) (40 mg) was dissolved in 1.5 mL DMF for 20 min, then 4 mL deionized water was added slowly to the above solution. After stirring for another 2 h, the mixture was dialyzed against deionized water for 36 h (3500 Da), and the water was replaced every 4 h. The obtained solution was filtered through 0.45 μm microfilter and lyophilized. For drug-loaded micelles, the preparation procedure was under a dark environment during the entire time period. PEG-*b*-poly(DPA-*co*-DTM) (40 mg) and DOX (15 mg) were dissolved together in 2 mL DMF by stirring for 30 min, then 5 mL deionized water was added slowly to the above solution. After again stirring for 2 h, the mixture was filtered to remove precipitated DOX and was dialyzed against deionized water for 36 h (3500 Da), and the water was replaced every 4 h. The obtained solution was then lyophilized. In addition, for PEG-*b*-poly(DBA-*co*-DTM) micelle and DOX-loaded PEG-*b*-poly(DBA-*co*-DTM) micelle, the preparation methods were as the same. PEG-*b*-poly (DPA-*co*-DTM) micelles, PEG-*b*-poly(DBA-*co*-DTM) micelles, DOX-loaded PEG-*b*-poly(DPA-*co*-DTM) micelles and DOX-loaded PEG-*b*-poly(DBA-*co*-DTM) micelles are referred to **P1** micelles, **P2** micelles, DOX-loaded **P1** micelles, and DOX-loaded **P2** micelles, respectively, in the following sections.

2.6. In vitro drug release from DOX-loaded micelles

Freeze-dried DOX-loaded **P1** micelles and DOX-loaded **P2** micelles were dispersed into 0.1 M citric acid-sodium phosphate buffer solution (pH 7.4 and pH 6.0 for DOX-loaded **P1** micelles;

pH 7.4 and pH 5.0 for DOX-loaded **P2** micelles) and were transferred into the dialysis membrane (3500 Da) immersed in 50 mL citric acid-sodium phosphate buffer solution at 37 °C. At predetermined intervals, 3 mL external medium was collected and replaced with the same volume of fresh buffer solution. UV–vis absorption at the wavelength of 488 nm was employed to assay the DOX content to determine the drug loading efficiency (DLE), the drug loading content (DLC), and the DOX release rate. In addition, the release experiments were conducted in triplicate. The DLE (%) and DLC (%) were calculated as

$$\mathrm{DLE(wt\%)} = (\text{weight of loaded drug/weight of drug in feed}) \times 100\%$$

$$\mathrm{DLC(wt\%)} = (\text{weight of loaded drug/weight of polymer and drug}) \times 100\%$$

2.7. Cellular uptake

A549 cells in DMEM supplemented with 10% FBS were seeded into two 6-well plates at a density of 1×10^4 cells per well and were cultured for 24 h at 37 °C in CO_2/air (5/95, v/v). The prepared **P1** micelles, **P2** micelles, DOX-loaded **P1** micelles and DOX-loaded **P2** micelles were added at a final DTM group concentration of 10 μg mL^{-1}. After further incubation for 15 min, 45 min, or 3 h, these cells were washed three times with PBS. Then, the cells were fixed for 10 min. Finally, the cells were washed with PBS again and were observed with a confocal microscope.

2.8. In vitro cytotoxicity assay

The *in vitro* cytotoxicity of **P1** micelles and the viability of A549 cells treated with free DOX and DOX-loaded **P1** micelles were evaluated by the Cell Counting Kit (CCK-8) assay. A549 cells in DMEM supplemented with 10% FBS were seeded into 96-well plates at a density of 1×10^4 cells per well and were cultured for 24 h at 37 °C in CO_2/air (5/95, v/v). Then, the cells were cultured with medium containing various concentrations of **P1** micelles from 25 to 200 μg mL^{-1}, as well as free DOX and DOX-loaded **P1** micelles with a final DOX concentration ranging from 1 to 20 μg mL^{-1}. After the cells were incubated for 24 h or 48 h, 10 μL CCK-8 solution was added to each well, and the cells were incubated for another 2 h at 37 °C. The cell viability was determined by a microplate reader of absorbance at 450 nm. The *in vitro* cytotoxicity of **P2** micelles and the viability of A549 cells treated with free DOX and DOX-loaded **P2** micelles were evaluated by the same methods.

2.9. In vitro apoptosis

For the apoptosis assay, A549 cells were cultured in a six-well plate and were further grown for 24 h. Then, the cells were treated with pure **P1** micelles, **P2** micelles, DOX-loaded **P1** and DOX-loaded **P2** micelles. After 24 h of incubation, all attached and floating cells were collected and mixed with 50 of Muse™ annexin V & Dead Cell Reagent for 10 min in the dark at room temperature. Then, the samples were detected by a Muse Cell Analyzer.

3. Results and discussion

3.1. Synthesis and characterization of block copolymers

The fluorescent and pH-responsive amphiphilic block copolymers of PEG-*b*-poly(DPA-*co*-DTM) and PEG-*b*-poly(DBA-*co*-DTM) were synthesized according to Scheme 1. DTM was first modified into monomer DTM-MA, and then the macroinitiator PEG-Br initiated the atom transfer radical polymerization (ATRP) of DTM-MA and DPA-MA or DBA-MA to obtain block copolymers with PEG as the hydrophilic parts and fluorescent DTMs incorporated into pH-responsive parts. The lengths of the PDPA segments and the

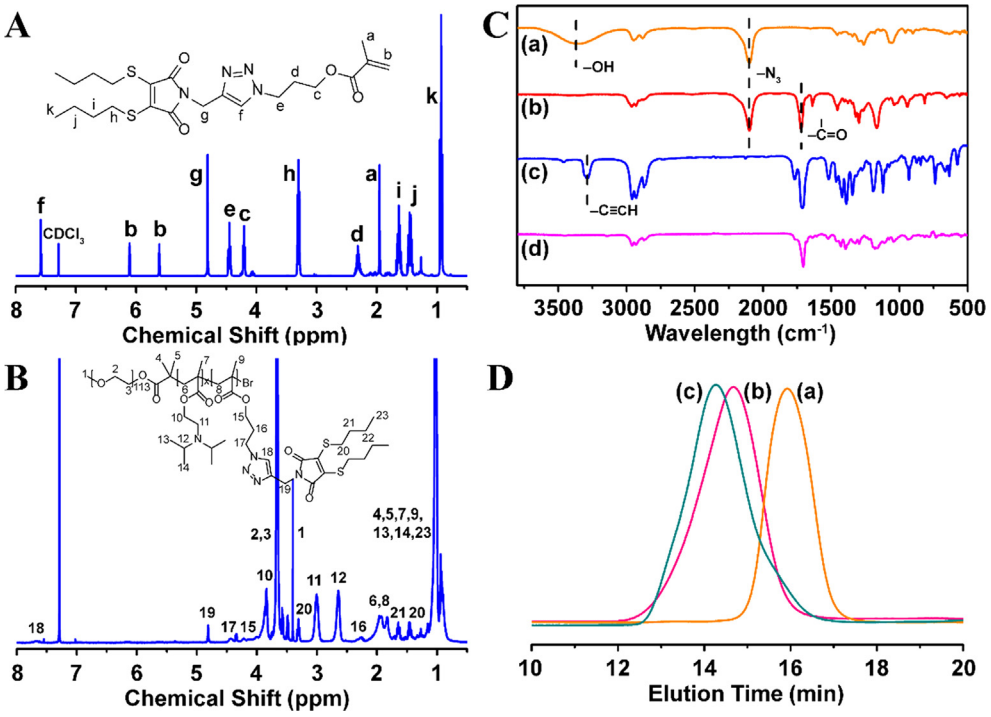

Fig. 1. ^{1}H NMR spectra of DTM-MA (A) and PEG_{113}-*b*-poly(DPA_{80}-*co*-DTM_5) (B) in chloroform; FT-IR spectra of (a) AzPOH, (b) AzPMA, (c) alkyne-DTM and (d) DTM-MA (C); GPC traces of (a) PEG-Br, (b) PEG_{113}-*b*-poly(DPA_{80}-*co*-DTM_5), (c) PEG_{113}-*b*-poly(DBA_{80}-*co*-DTM_5) (D).

PDBA segments in block copolymers were tuned by controlling the polymerization process.

The stepwise synthesis of monomer DTM-MA could be verified in the ^{1}H NMR and FT-IR results. ^{1}H NMR confirmed the synthesis of AzPMA by the disappearance of the signal at 2.0 ppm (hydroxyl group) and the onsite of double bond peaks at 5.6 ppm and 6.1 ppm (Figs. S1–S2). The triazole group at 7.6 ppm, which appeared in the ^{1}H NMR, proved the successful synthesis of DTM-MA (Fig. 1A and S3). The infrared spectra (Fig. 1C) evidenced the synthesis of AzPMA from the disappearance of the hydroxyl group peak at 3334 nm^{-1}, the onsite of the ketone group at 1720 nm^{-1}, and the formation of DTM-MA from the disappearances of the alkynyl group peak at 3189 nm^{-1} and the N_3 group at 2100 nm^{-1}.

We then characterized the chemical structure of the synthesized block copolymers. For PEG_{113}-*b*-poly(DPA_{80}-*co*-DTM_5) (Fig. 1B), the peaks at 3.0 ppm and 2.6 ppm were associated with the methylene and methine next to the nitrogen atom in the PDPA, and the peak at 7.6 ppm referred to the triazole group in the PDTM. For PEG_{113}-*b*-poly(DBA_{80}-*co*-DTM_5) (Fig. S4), the peaks at 2.5–2.7 ppm referred to the methylene next to the nitrogen atom in the PDBA, and the peak at 7.6 ppm referred to the triazole group in the PDTM. The molecular weight results that were measured by GPC and NMR are shown in Table S1 and Fig. 1D. The M_n of polymer PEG_{113}-*b*-poly(DPA_{80}-*co*-DTM_5) and PEG_{113}-*b*-poly(DBA_{80}-*co*-DTM_5) were 24.3 kDa and 26.1 kDa, respectively, and the PDI were 1.28 and 1.21, respectively, which agreed well with the theoretical molecular weights results that were calculated by ^{1}H NMR. Then, the PEG_{113}-*b*-poly(DPA_{80}-*co*-DTM_5) and PEG_{113}-*b*-poly(DBA_{80}-*co*-DTM_5) copolymers were named **P1** and **P2** for subsequent following measurements.

Particle size is an important property of polymeric micelles for drug delivery and release. For the designed amphiphilic block copolymers **P1** and **P2**, the hydrophilic segment PEG is the shell and the hydrophobic segments P(DPA-*co*-DTM) or P(DBA-*co*-DTM) are the cores of the micelle. The DLS results of intensity indicated that the size distributions were approximately 28 ± 8 nm and 37 ± 6 nm for **P1** and **P2** micelles, whereas the cryo-TEM results showed smaller size distributions of approximately 16 ± 2 nm and 27 ± 4 nm (Fig. 2a and b). After loading DOX into micelles, the cryo-TEM observations for DOX-loaded **P1** micelles and DOX-loaded **P2** micelles revealed that the size distributions are approximately 27 ± 5 nm and 36 ± 8 nm, respectively, which were also smaller than the DLS results (39 ± 10 nm for DOX-loaded **P1** micelles and 47 ± 15 nm for DOX-loaded **P2** micelles) (Fig. 2c and d). After encapsulating the drug into the micelles, the size distributions of DLS showed a ~30% increase for DOX-loaded **P1** micelles and a ~21% increase for DOX-loaded **P2** micelles. However, both

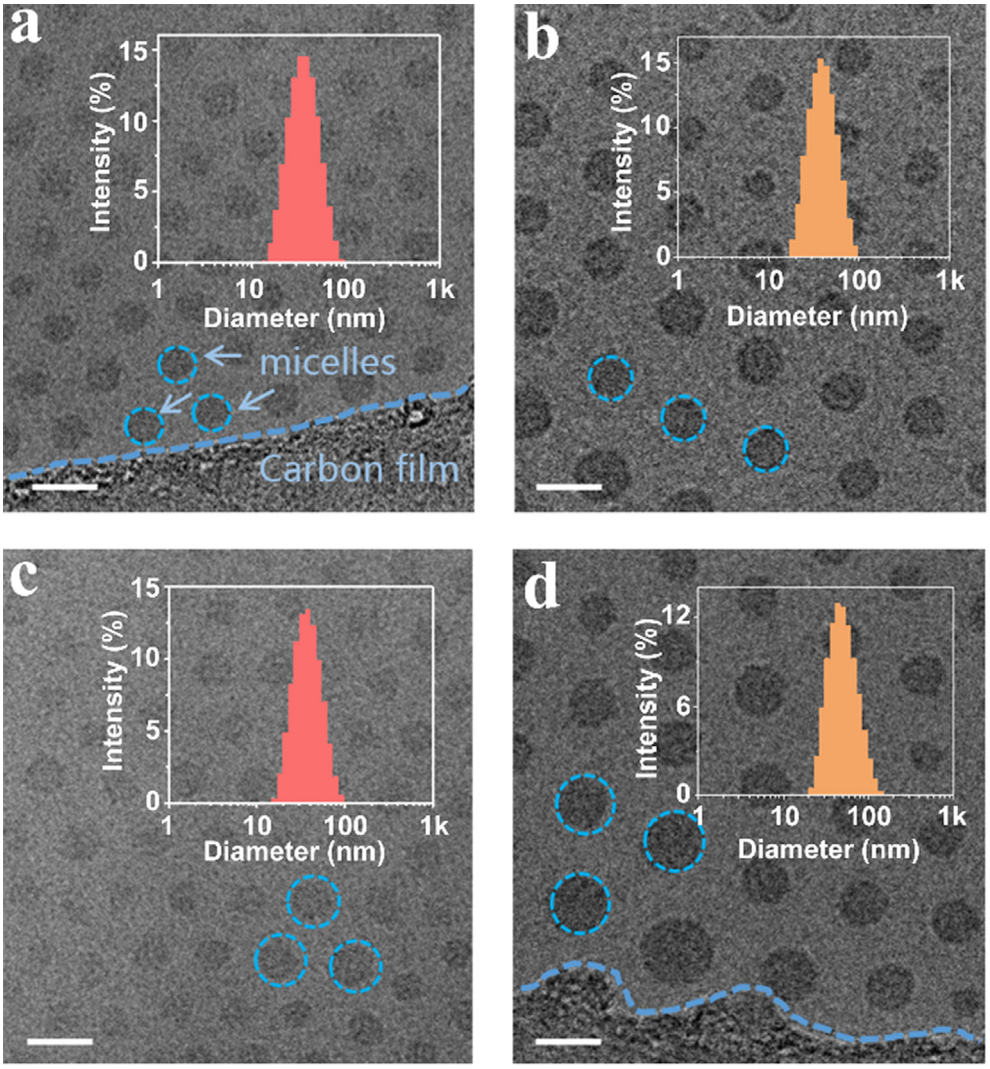

Fig. 2. Cryo-TEM images of (a) **P1** micelles, (b) **P2** micelles, (c) DOX-loaded **P1** micelles, (d) DOX-loaded **P2** micelles. (scale bar = 30 nm) Inset: DLS characterization.

DOX-loaded micelles were within 200 nm, which therefore could penetrate and accumulate in tumor tissues through an enhanced permeability and retention (EPR) effect [42,43].

As is well known, the PDPA and PDBA polymers hold pH-responsive properties, with a sharp pH responsive transition from hydrophobic to hydrophilic response to pH changes from 7.4 to 6.3 (for PDPA) and from 7.4 to 5.4 (for PDBA), respectively [25]. To assess the micelle stability of **P1** micelles and **P2** micelles at different pH levels, we measured the size changes of micelles (Fig. 3a, c and S6) in a citric acid-sodium phosphate buffer solution with a polymer concentration of 1 mg mL^{-1} at different pH values. At pH 7.4, the observed hydrodynamic diameters of both micelles were approximately 30–40 nm and remained constant over 36 h. However, the sizes of both micelles showed obvious changes at pH values of 6.0 and 5.0, which could be attributed to the charge transitions of the hydrophobic segments with tertiary amines at a low pH, thus yielding micelle dissociation [25,44]. This characteristic was also confirmed by cryo-TEM when the pH was reduced to 6.0 and 5.0, and there were almost no spherical nanoparticles with normal sizes after 30 min incubation (Fig. 3b and d).

3.2. In vitro drug release

The recent studies revealed that the pH value in tumor issues is slightly lower than that in normal tissues, which is a benefit for targeting applications, and the intracellular pH value is lower than extracellular, which is typically 5.9–6.2 in early endosomes and 5.0–5.5 in late endosomes/lysosomes [19–21]. During the *in vitro* drug releasing characterization, the analytical results from DLC and DLE equations indicated that the drug-loading content and encapsulation efficiency of the DOX-loaded **P1** micelles were 22.5% and 92.1%, respectively, and those of DOX-loaded **P2** micelles were 16.1% and 76.3%, respectively. Therefore, the *in vitro* drug release experiments were evaluated in a corresponding responsive pH range, i.e., pH 7.4 and 6.0 for DOX-loaded **P1** micelles and pH 7.4 and 5.0 for DOX-loaded **P2** micelles.

At a pH value of 7.4 (Fig. 4), the DOX-releasing efficiencies remained relatively stable, with less than 30% from both the DOX-loaded **P1** micelles and DOX-loaded **P2** micelles in 36 h. At pH 6.0, we observed an acceleration of the drug release for DOX-loaded **P1** micelles; approximately 53% of the loaded DOX were released in the first 12 h, which climbed up to 72% at 36 h. Similarly, approximately 42% of DOX was released from DOX-loaded **P2** micelles in the first 12 h, and the release rate reached 69% at 36 h. It was quite obvious that our micelles presented accelerated drug release behaviour at lower corresponding pH values.

3.3. Fluorescence spectroscopy

When two alkyl thiol groups are added into a nonfluorescent dibromomaleimide molecule, a dithiomaleimide molecule will be formulated with a strong fluorescence signal [30]. The mechanism

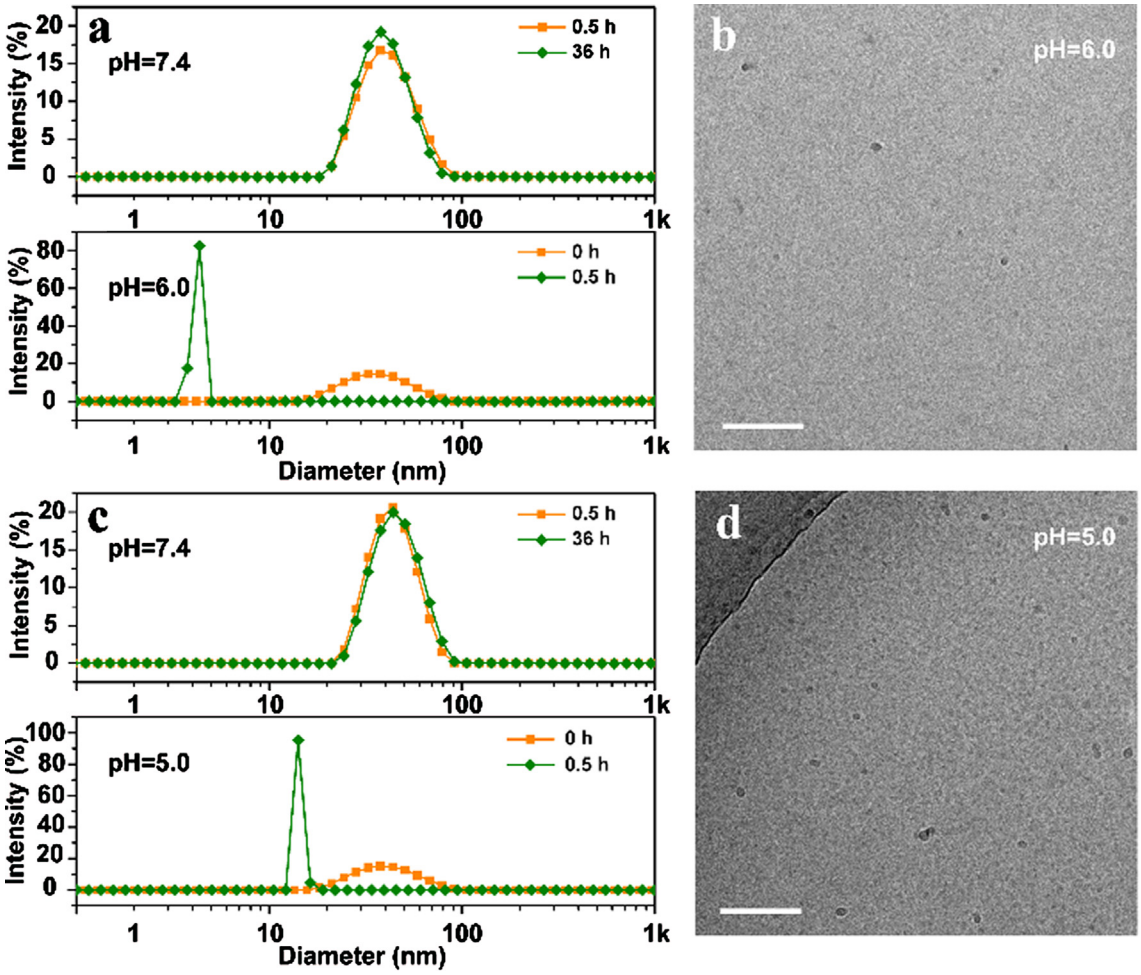

Fig. 3. (a) Size change for **P1** micelles at pH = 7.4 and pH = 6.0, within 0.1 M citric acid-sodium phosphate buffer solution (37 °C); (b) cryo-TEM images of **P1** micelles at pH = 6.0 (scale bar = 50 nm); (c) size change for **P2** micelles at pH = 7.4 and pH = 5.0, within 0.1 M citric acid-sodium phosphate buffer solution (37 °C); (d) cryo-TEM images of **P2** micelles at pH = 5.0 (scale bar = 50 nm).

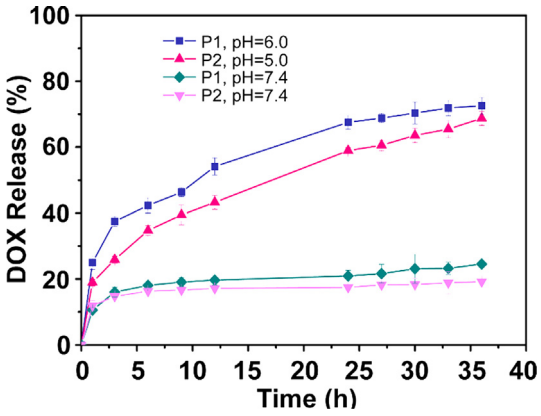

Fig. 4. DOX release profiles from DOX-loaded micelles in a citric acid-sodium phosphate buffer solution (0.1 M, 37 °C). Data are presented as the mean ± SD (n = 3).

that was previously reported by other researchers was that thiol groups can saturate the C=C double bond of the maleimide, subsequently eliminating the quenching of fluorophore and eventually making the fluorophore excitative [45]. The above mechanism also applies to our **P1** and **P2** copolymers.

We assessed the fluorescence property of our samples. Under the methanol environment (Fig. 5a), the maximum excitation wavelength of both **P1** and **P2** copolymers were observed at 405 nm, and the maximum emission wavelength was 550 nm, which was in a good agreement with that of the DTM-MA monomer. In DI-water (Fig. 5b), the maximum excitation wavelength showed no shift; however, there was a slight shift from 550 nm to 520 nm for the maximum emission wavelength, which is known as a solvatochromic emission with a blueshift when changing solvent polarity [45]. The solvents affected not only the emission wavelength but also the intensity of the emission wavelength. When the **P1** and **P2** copolymers were dissolved in the H_2O/DMF mixture with different water fractions (f_w), the samples exhibited proportional fluorescence quenching, and the emission intensity decreased to a certain value instead of fully quenching (Figs. S7–S8). This obvious fluorescence quenching might be greatly caused by hydrogen bonding between the water and carbonyl moiety of the DTM group [45,46]. Then, after exposure under a UV light, our samples exhibited visible green fluorescence (Fig. 5c).

3.4. Cellular uptake and cytotoxicity

The cellular uptake experiments were performed for both **P1** and **P2** micelles against A549 cells to understand the dynamic fluorescence behaviour in a practical cell environment [47]. For pure micelles, a weak green fluorescence signal appeared in A549 cells at an incubation duration of 15 min, and enhanced green fluorescence intensities were discovered at 45 min and 3 h (Fig. S9). For DOX-loaded **P1** and **P2** micelles (Fig. 6), no fluorescence signals could be found at 15 min, as no drug-loaded copolymers entered

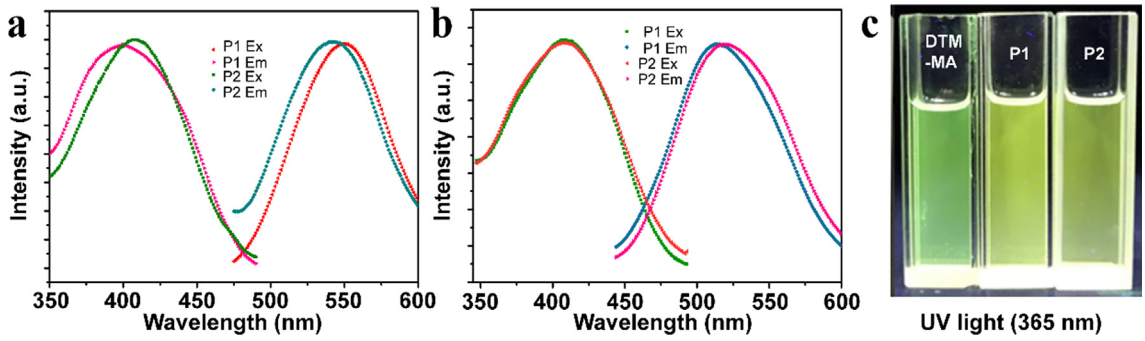

Fig. 5. Fluorescence excitation and emission spectra of both **P1** and **P2** copolymers in (a) methanol, and (b) deionized water. (c) Photographs of DTM-MA (2×10^{-5} M), **P1** copolymer (0.3 mg ml^{-1}) and **P2** copolymer (0.3 mg ml^{-1}) dissolved in methanol, taken under UV light (365 nm).

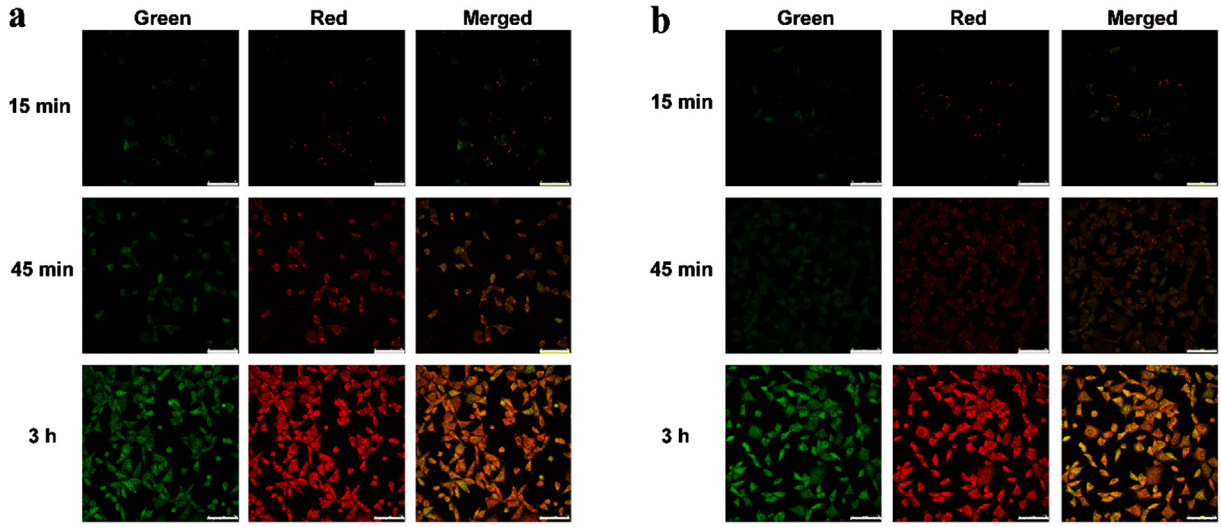

Fig. 6. Fluorescence microscopy images of A549 cells after incubation of DOX loaded (a) **P1** and (b) **P2** micelles for 15 min, 45 min and 3 h. (Scale bar = 75 μm).

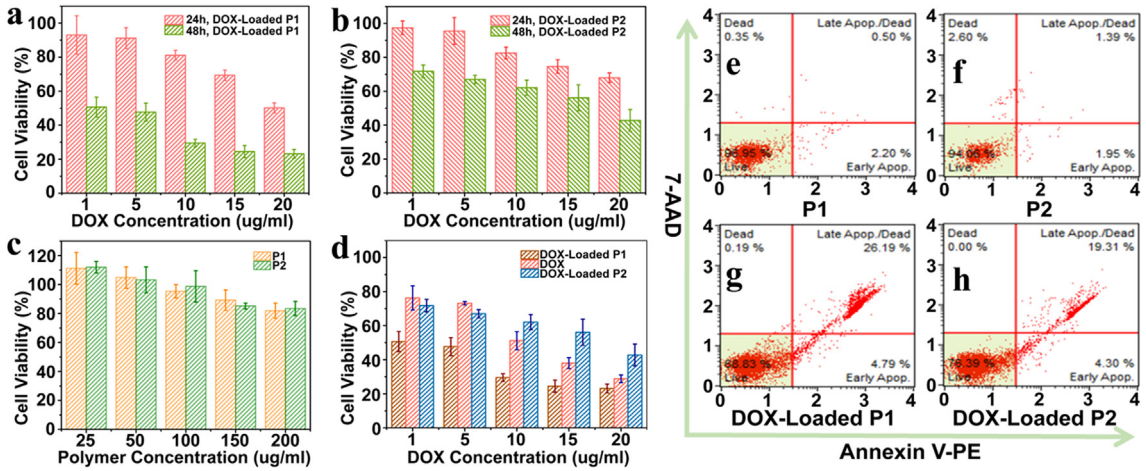

Fig. 7. Cell viability results with (a) DOX-loaded **P1** micelles and (b) DOX-loaded **P2** micelles for 24 h and 48 h incubations at varying DOX concentrations, (c) **P1** micelles and **P2** micelles after 24 h incubation, (d) free DOX, DOX-loaded **P1** and DOX-loaded **P2** micelles for 48 h incubation at varying equivalent DOX concentrations (n = 3). A549 Cell apoptosis analysis induced by (e) **P1** micelles, (f) **P2** micelles, (g) DOX-loaded **P1** micelles, (h) DOX-loaded **P2** micelles for 24 h incubation.

into the A549 cells yet. At incubation durations of 45 min and 3 h, clear fluorescence signals were observed, which implied successful engagement between the A549 cells and the drug-loaded micelles. The intracellular distribution of copolymers and DOX indicated the clear potential to use these materials as fluorescent probes.

To determine the biocompatibility and cytotoxicity of pure micelles, free DOX and DOX-loaded micelles were assessed in the cell viability experiments by using the Cell Counting Kit 8 (CCK-8) assay. In Fig. 7a and b, the DOX-loaded **P1** and **P2** micelles presented an efficient antitumor activity against A549 cells after incubation durations of 24 h and 48 h, respectively. Concentration- and time-dependent toxicities were reflected by the reduction of cell viabilities when the incubation duration time increased and the DOX concentration increased from 1 to 20 μg mL^{-1}. In Fig. 7c, the results for pure **P1** and **P2** micelles suggested an excellent biocompatibility as nearly 85% cells with fluorescent micelles survived when testing concentrations up to 200 μg mL^{-1}.

The antitumor efficiencies for DOX and DOX-loaded micelles were evaluated by comparing the cell viability results after a fixed incubation period of 48 h, as shown in Fig. 7d. DOX-loaded **P1** micelles showed the lowest cell viability towards A549 cells with all DOX concentrations, because the PDPA segment in the **P1** copolymer, responding to a pH of 6.3, would immediately release DOX when micelles entered into the tumor cells that were occupied by early endosomes (pH = 6.3), thus resulting in an effective longer drug toxicity to kill tumor cells. Due to the lower pH responsive transition (pH = 5.4) from PDBA, DOX-loaded **P2** micelles needed to reach late endosomes/lysosomes (pH = 5.4) to release the DOX. Compared to reaching early endosomes, reaching late endosomes/lysosomes took more time by intracellular diffusion constant-controlled travel, thus leading to low antitumor efficiency. Similarly, the results from free DOX also indicated low antitumor efficiency, which resulted from diffusion-controlled transportation from the extracellular matrix to the intracellular system for the drug [48].

To further investigate the biocompatibility of copolymers and the cytotoxicity of DOX-loaded micelles, an Annexin V-PE/7-AAD apoptosis detection assay was used. In Fig. 7e–h, the total apoptotic rate (sum of the early apoptotic, late apoptotic and dead ratios) of A549 cells was determined to be 3.05% (**P1** micelles), 5.94% (**P2** micelles), 31.17% (DOX-loaded **P1** micelles), and 23.61% (DOX-loaded **P2** micelles) after an incubation duration of 24 h. Pure micelles had little toxicity towards A549 cells as more live cells were detected, which agreed well with the results from CCK-8 assay testing. In contrast, more apoptosis was observed for DOX-loaded micelles, for which an apoptosis ratio of 26.19% was found for DOX-loaded **P1** micelles, and an apoptosis ratio of 19.31% was found for DOX-loaded **P2** micelles. These results are in good agreement with the cytotoxicity profiles, in which DOX-loaded **P1** micelles had a higher antitumor efficiency toward A549 cells than did DOX-loaded **P2** micelles.

4. Conclusions

In summary, we successfully developed novel fluorescence pH-responsive block copolymers with robust fluorescence performance that could resist solvent intervention. DOX-loaded **P1** micelles showed the best antitumor effect by immediately releasing DOX once they entered the tumor cells as a result of responding to the regional pH level (pH = 6.3). This early drug release not only extends the working time for the drug but also kinetically enhances the toxicity to kill cancer cells. Moreover, both PEG-*b*-Poly(DPA-*co*-DTM) and PEG-*b*-Poly(DBA-*co*-DTM) copolymers show excellent biocompatibility, as nearly 85% of cells with these fluorescent micelles survive when the testing concentration increases to 200 μg mL^{-1}. This was the first time that the fluorescent DTM group was used to cooperate with pH-responsive drug delivery system, and the copolymer showed great fluorescence performance, which implied a great candidate for diagnostic imaging. In addition, compared to the traditional drug delivery system with low drug loading, broad pH response and no fluorescence, this work presented higher drug loading, a sharp pH response to endosomes and great fluorescence performance [25,26,39,43]. With the superior fluorescence property and sensitive pH-responsive drug releasing property, we expect that technology employing these fluorescent polymeric micelles targeting specific endocytic organelles could have potential applications in biomedical and clinical therapeutics.

Declaration of Competing Interest

There are no conflicts to declare.

Acknowledgements

This work was financially supported by the National Natural Science Foundation of China (21604065/21374089), Shaanxi

Natural Science Funds for Distinguished Young Scholars (2018JC-008), Innovation Foundation for Doctor Dissertation of Northwestern Polytechnical University (CX201837), Fundamental Research Funds for the Central Universities (3102018jgc010), China Postdoctoral Science Foundation (2018T111098/2017M613211) and the Engineering and Physical Sciences Research Council (EPSRC) grant-EP/N007921/1.

Appendix A. Supplementary material

Supplementary data to this article can be found online at https://doi.org/10.1016/j.jcis.2019.05.074.

References

[1] M. Gao, F.B. Yu, C.J. Lv, J. Choo, L.X. Chen, Fluorescent chemical probes for accurate tumor diagnosis and targeting therapy, Chem. Soc. Rev. 46 (2017) 2237–2271.
[2] B.R. Smith, S.S. Gambhir, Nanomaterials for in vivo imaging, Chem. Rev. 117 (2017) 901–986.
[3] B. Pelaz, C. Alexiou, R.A. Alvarez-Puebla, F. Alves, A.M. Andrews, S. Ashraf, L.P. Balogh, L. Ballerini, A. Bestetti, Diverse applications of nanomedicine, ACS Nano 11 (2017) 2313–2318.
[4] L. Yuan, W.Y. Lin, K.B. Zheng, L.W. He, W.M. Huang, Far-red to near infrared analyte-responsive fluorescent probes based on organic fluorophore platforms for fluorescence imaging, Chem. Soc. Rev. 42 (2013) 622–661.
[5] O.S. Wolfbeis, An overview of nanoparticles commonly used in fluorescent bioimaging, Chem. Soc. Rev. 44 (2015) 4743–4768.
[6] Y.M. Yang, Q. Zhao, W. Feng, F.Y. Li, Luminescent chemodosimeters for bioimaging, Chem. Rev. 113 (2013) 192–270.
[7] M. Vendrell, D.T. Zhai, J.C. Er, Y.T. Chang, Combinatorial strategies in fluorescent probe development, Chem. Rev. 112 (2012) 4391–4420.
[8] D.L. Wang, T.Y. Zhao, X.Y. Zhu, D.Y. Yan, W.X. Wang, Bioapplications of hyperbranched polymers, Chem. Soc. Rev. 44 (2015) 4023–4071.
[9] R.Y. Zhan, Y.T. Pan, P.N. Manghnani, B. Liu, AIE polymers: synthesis, properties, and biological applications, Macromol. Biosci. 17 (2017) 1600433–1600452.
[10] R.R. Hu, N.L.C. Leung, B.Z. Tang, AIE macromolecules: syntheses, structures and functionalities, Chem. Soc. Rev. 43 (2014) 4494–4562.
[11] B. Guo, X.L. Cai, S.D. Xu, S.M.A. Fateminia, J. Liu, J. Liang, G.X. Feng, W.B. Wu, B. Liu, Decoration of porphyrin with tetraphenylethene: converting a fluorophore with aggregation-caused quenching to aggregation-induced emission enhancement, J. Mater. Chem. B 4 (2016) 4690–4695.
[12] A.M. Derfus, W.C.W. Chan, S.N. Bhatia, Probing the cytotoxicity of semiconductor quantum dots, Nano Lett. 4 (2004) 11–18.
[13] R.A. Hardman, A toxicologic review of quantum dots: toxicity depends on physicochemical and environmental factors, Environ. Health. Perspect. 114 (2006) 165–172.
[14] J.H. Kim, K. Park, H.Y. Nam, S. Lee, K. Kim, I.C. Kwon, Polymers for bioimaging, Prog. Polym. Sci. 32 (2007) 1031–1053.
[15] Y.J. Zhao, Y. Wu, B. Xue, X. Jin, X.Y. Zhu, Novel target NIR-fluorescent polymer for living tumor cell imaging, Polym. Chem. 10 (2019) 77–85.
[16] Y. Hu, S. Mignani, J.P. Majoral, M.W. Shen, X.Y. Shi, Construction of iron oxide nanoparticle-based hybrid platforms for tumor imaging and therapy, Chem. Soc. Rev. 47 (2018) 1874–1900.
[17] X.G. Liu, M. Wu, Q.L. Hu, H.Z. Bai, S.Q. Zhang, Y.Q. Shen, G.P. Tang, Y. Ping, Precise imaging-guided cancer therapy and real-time pharmacokinetic monitoring, ACS Nano 10 (2016) 11385–11396.
[18] A. Gianella, P.A. Jarzyna, V. Mani, S. Ramachandran, C. Calcagno, J. Tang, B. Kann, W.J.R. Dijk, V.L. Thijssen, A.W. Griffioen, G. Storm, Z.A. Fayad, W.J.M. Mulder, Multifunctional nanoemulsion platform for imaging guided therapy evaluated in experimental cancer, ACS Nano 5 (2011) 4422–4433.
[19] J.Y. Han, K. Burgess, Fluorescent indicators for intracellular pH, Chem. Rev. 110 (2010) 2709–2728.
[20] J.T. Hou, W.X. Ren, K. Li, J. Seo, A. Sharma, X.Q. Yu, J.S. Kim, Fluorescent bioimaging of pH: from design to applications, Chem. Soc. Rev. 46 (2017) 2076–2090.
[21] L.Y. Fu, P. Yuan, Z. Ruan, L. Liu, T.W. Li, L.F. Yan, Ultra-pH-sensitive polypeptide micelles with large fluorescence off/on ratio in near infrared range, Polym. Chem. 8 (2017) 1028–1038.
[22] M.L. Wei, Y.F. Gao, X. Li, M.J. Serpe, Stimuli-responsive polymers and their applications, Polym. Chem. 8 (2017) 127–143.
[23] S.L. Li, K.L. Hu, W.P. Cao, Y. Sun, W. Sheng, F. Li, Y. Wu, X.J. Liang, pH-Responsive biocompatible fluorescent polymer nanoparticles based on phenylboronic acid for intracellular imaging and drug delivery, Nanoscale 6 (2014) 13701–13709.
[24] G. Kocak, C. Tuncer, V. Bütün, pH-Responsive polymers, Polym. Chem. 8 (2017) 144–176.
[25] K.J. Zhou, Y.G. Wang, X.N. Huang, K. Luby-Phelps, B.D. Sumer, J.M. Gao, Tunable, ultrasensitive pH-responsive nanoparticles targeting specific endocytic organelles in living cells, Angew. Chem. Int. Ed. 50 (2011) 6109–6114.
[26] K.J. Zhou, H.M. Liu, S.R. Zhang, X.N. Huang, Y.G. Wang, G. Huang, B.D. Sumer, J. M. Gao, Multicolored pH-tunable and activatable fluorescence nanoplatform responsive to physiologic pH stimuli, J. Am. Chem. Soc. 134 (2012) 7803–7811.
[27] X.P. Ma, Y.G. Wang, T. Zhao, Y. Li, L.C. Su, Z.H. Wang, G. Huang, B.D. Sumer, J.M. Gao, Ultra-pH-sensitive nanoprobe library with broad pH tunability and fluorescence emissions, J. Am. Chem. Soc. 136 (2014) 11085–11092.
[28] Y.G. Wang, C.S. Wang, Y. Li, G. Huang, T. Zhao, X.P. Ma, Z.H. Wang, B.D. Sumer, M.A. White, J.M. Gao, Digitization of endocytic pH by hybrid ultra-pH-sensitive nanoprobes at single-organelle resolution, Adv. Mater. 29 (2017) 1603794–1603802.
[29] X.D. Xu, J. Wu, Y.L. Liu, M. Yu, L.L. Zhao, X. Zhu, S. Bhasin, Q. Li, E. Ha, J.J. Shi, O. C. Farokhzad, Ultra-pH-responsive and tumor-penetrating nanoplatform for targeted siRNA delivery with robust anti-cancer efficacy, Angew. Chem. Int. Ed. 55 (2016) 7091–7094.
[30] M.P. Robin, P. Wilson, A.B. Mabire, J.K. Kiviaho, J.E. Raymond, D.M. Haddleton, R.K. O'Reilly, Conjugation-induced fluorescent labeling of proteins and polymers using dithiomaleimides, J. Am. Chem. Soc. 135 (2013) 2875–2878.
[31] A.B. Mabire, M.P. Robin, H. Willcock, A. Pitto-Barry, N. Kirby, R.K. O'Reilly, Dual effect of thiol addition on fluorescent polymeric micelles: ON-to-OFF emissive switch and morphology transition, Chem. Commun. 50 (2014) 11492–11495.
[32] M.P. Robin, A.B. Mabire, J.C. Damborsky, E.S. Thom, U.H. Winzer-Serhan, J.E. Raymond, R.K. O'Reilly, New functional handle for use as a self-reporting contrast and delivery agent in nanomedicine, J. Am. Chem. Soc. 135 (2013) 9518–9524.
[33] M.P. Robin, R.K. O'Reilly, Fluorescent and chemico-fluorescent responsive polymers from dithiomaleimide and dibromomaleimide functional monomers, Chem. Sci. 5 (2014) 2717–2723.
[34] M.P. Robin, J.E. Raymond, R.K. O'Reilly, One-pot synthesis of super-bright fluorescent nanogel contrast agents containing a dithiomaleimide fluorophore, Mater. Horiz. 2 (2015) 54–59.
[35] M.P. Robin, S.A.M. Osborne, Z. Pikramenou, J.E. Raymond, R.K. O'Reilly, Fluorescent block copolymer micelles that can self-report on their assembly and small molecule encapsulation, Macromolecules 49 (2016) 653–662.
[36] M.W. Jones, R.A. Strickland, F.F. Schumacher, S. Caddick, J.R. Baker, M.I. Gibson, D.M. Haddleton, Highly efficient disulfide bridging polymers for bioconjugates from radical-compatible dithiophenol maleimides, Chem. Commun. 48 (2012) 4064–4066.
[37] L. Castañeda, A. Maruani, F.F. Schumacher, E. Miranda, V. Chudasama, K.A. Chester, J.R. Baker, M.E.B. Smith, S. Caddick, Acid-cleavable thiomaleamic acid linker for homogeneous antibody-drug conjugation, Chem. Commun. 49 (2013) 8187–8189.
[38] H. Wang, M. Xu, M.H. Xiong, J.J. Cheng, Reduction-responsive dithiomaleimide-based nanomedicine with high drug loading and FRET-indicated drug release, Chem. Commun. 51 (2015) 4807–4810.
[39] T. Bai, J.J. Du, J.X. Chen, X. Duan, Q. Zhuang, H. Chen, J. Kong, Reduction-responsive dithiomaleimide-based polymeric micelles for controlled anti-cancer drug delivery and bioimaging, Polym. Chem. 8 (2017) 7160–7168.
[40] O. Bertrand, B. Ernould, F. Boujioui, A. Vladb, J.F. Gohy, Synthesis of polymer precursors of electroactive materials by SET-LRP, Polym. Chem. 6 (2015) 6067–6072.
[41] Z.F. Jia, V.A. Bobrin, N.P. Truong, M. Gillard, M.J. Monteiro, Multifunctional nanoworms and nanorods through a one-step aqueous dispersion polymerization, J. Am. Chem. Soc. 136 (2014) 5824–5827.
[42] Q.F. Ban, T. Bai, X. Duan, J. Kong, Noninvasive photothermal cancer therapy nanoplatforms via integrating nanomaterials and functional polymers, Biomater. Sci. 5 (2017) 190–210.
[43] X. Duan, T. Bai, J.J. Du, J. Kong, One-pot synthesis of glutathione-responsive amphiphilic drug self-delivery micelles of doxorubicin-disulfide-methoxy polyethylene glycol for tumor therapy, J. Mater. Chem. B 6 (2018) 39–43.
[44] M.M. Huang, K.J. Zhao, L. Wang, S.Q. Lin, J.J. Li, J.B. Chen, C.G. Zhao, Z.S. Ge, Dual stimuli-responsive polymer prodrugs quantitatively loaded by nanoparticles for enhanced cellular internalization and triggered drug release, ACS Appl. Mater. Interfaces 8 (2016) 11226–11236.
[45] A.B. Mabire, M.P. Robin, W.D. Quan, H. Willcock, V.G. Stavros, R.K. O'Reilly, Aminomaleimide fluorophores: a simple functional group with bright, solvent dependent emission, Chem. Commun. 51 (2015) 9733–9736.
[46] Q.H. Zhu, Z.W. Ye, W.J. Yang, X.T. Cai, B.Z. Tang, One-pot synthesis and structure-property relationship of aminomaleimides: fluorescence efficiencies in monomers and aggregates easily tuned by switch of aryl and alkyl, J. Org. Chem. 82 (2017) 1096–1104.
[47] L.L. Wu, X.L. Li, Y.F. Ling, C.S. Huang, N.Q. Jia, Morpholine derivative-functionalized carbon dots-based fluorescent probe for highly selective lysosomal imaging in living cells, ACS Appl. Mater. Interfaces 9 (2017) 28222–28232.
[48] D.W. Li, Y.Z. Bu, L.N. Zhang, X. Wang, Y.Y. Yang, Y.P. Zhuang, F. Yang, H. Shen, D. C. Wu, Facile construction of pH- and redox-responsive micelles from a biodegradable poly(β-hydroxyl amine) for drug delivery, Biomacromolecules 17 (2016) 291–300.